Published in final edited form as:
Circulation. 2011 September 13; 124(11 Suppl): S81–S96. doi:10.1161/CIRCULATIONAHA.110.011163.

Rigid, Complete Annuloplasty Rings Increase Anterior Mitral Leaflet Strains in the Normal Beating Ovine Heart

Wolfgang Bothe, M.D.[*], **Ellen Kuhl, Ph.D.**[$,*], **John-Peder Escobar Kvitting, M.D. Ph.D.**[*], **Manuel K. Rausch, M.Sc.**[$], **Serdar Göktepe, Ph.D.**[$], **Julia C. Swanson, M.D.**[*], **Saideh Farahmandnia, M.D.**[*], **Neil B. Ingels Jr., Ph.D.**[#,*], and **D. Craig Miller, M.D.**[*]

[*]Department of Cardiothoracic Surgery, Stanford University School of Medicine, Stanford, California

[$]Department of Mechanical Engineering, Stanford University School of Engineering, Stanford, California

[#]Laboratory of Cardiovascular Physiology and Biophysics, Research Institute , Palo Alto Medical Foundation, Palo Alto, California

Abstract

Background—Annuloplasty ring or band implantation during surgical mitral valve repair perturbs mitral annular dimensions, dynamics and shape, which have been associated with changes in anterior mitral leaflet (AML) strain patterns and suboptimal long-term repair durability. We hypothesized that rigid rings with non-physiological 3-D shapes, but not saddle-shaped rigid rings or flexible bands, increase AML strains.

Methods and Results—Sheep had 23 radiopaque markers inserted: 7 along the anterior mitral annulus and 16 equally spaced on the AML. True-sized Edwards Cosgrove flexible, partial band (COS, n=12), rigid, complete St. Jude saddle-shaped annuloplasty ring (RSAR, n=12), Carpentier-Edwards Physio (PHYSIO, n=12), Edwards IMR ETlogix (ETL, n=11) and Edwards GeoForm (GEO, n=12) annuloplasty rings were implanted in a releasable fashion. Under acute open-chest conditions, four-dimensional marker coordinates were obtained using biplane videofluoroscopy along with hemodynamic parameters with the ring inserted and after release. Marker coordinates were triangulated and the largest maximum principal AML strains were determined during isovolumetric relaxation (IVR). No relevant changes in hemodynamics occurred. Compared to the respective Control state, strains increased significantly with RSAR, PHYSIO, ETL and GEO (0.14±0.05 *vs.* 0.16±0.05, p=0.024, 0.15±0.03 *vs.* 0.18±0.04, p=0.020, 0.11±0.05 *vs.* 0.14±0.05, p=0.042 and 0.13±0.05 *vs.* 0.16±0.05, p=0.009), but not with COS (0.15±0.05 vs. 0.15±0.04,p=0.973).

Conclusions—Regardless of 3-D shape, rigid, complete annuloplasty rings, but not a flexible, partial band, increased AML strains in the normal beating ovine heart. Clinical studies are needed

Address for Correspondence: D. Craig Miller, M.D. Department of Cardiothoracic Surgery Falk Cardiovascular Research Center Stanford University School of Medicine Stanford, California 94305-5247 001.650.725.3826 FAX 001.650.725.3846 dcm@stanford.edu.

DISCLOSURES D. Craig Miller, M.D.: Consultant, Medtronic CardioVascular Division; Consultant, St. Jude Medical, Inc.; PARTNER U.S. Pivotal Trial Executive Committee, Edwards Lifesciences (uncompensated); PARTNER U.S. pivot trial site PI, Edwards Lifesciences (uncompensated); Consultant, Abbott Vascular (MitraClip).

to determine if annuloplasty rings affect AML strains in patients, and, if so, whether ring-induced perturbations in leaflet strain states are linked to repair failure.

Keywords

mitral valve; physiology; mitral regurgitation; surgery

INTRODUCTION

Surgical mitral valve repair most commonly includes the insertion of an annuloplasty band or ring. While bands are flexible devices that spare the anterior, fibrous portion of the mitral annulus, rings encircle the entire annulus and may be either flexible, semi-rigid or rigid. Rigid rings are available in various shapes. The most commonly used ring (Carpentier-Edwards Physio) is flat, semi-rigid and D-shaped. Recently, saddle shaped, rigid, complete annuloplasty rings have been introduced (e.g. Saint Jude Medical RSAR, Medtronic Profile 3-D or Carpentier-Edwards Physio II) in order to account for the physiological 3-D shape of the mitral annulus [1, 2]. Furthermore, rigid rings with non-physiological shapes and dimensions have been designed specifically for patients with functional/ischemic mitral regurgitation (e.g. Edwards GeoForm and IMR ETLogix). These rings aim to counteract the main determinants of functional/ischemic mitral regurgitation (i.e. mitral annular dilatation, left ventricular (LV) dilatation and papillary muscle displacement) on an annular level via their specific designs, all of which include disproportionate annular septal-lateral downsizing [3]. While some studies demonstrate that such rings may reduce mitral leaflet strains in the diseased heart [4], other studies suggest that, by perturbing the natural mitral annular saddle-shape, disease-specific or non-physiologically shaped rings may increase leaflet strains in the normal heart [5-7]. Due to these results from *in vitro* measurements the authors speculate that such perturbations in mitral leaflet strain patterns could be associated with impaired long-term results after mitral valve repair [5-7]. Our goal was, therefore, to assess the effects of one flexible partial band and four different, complete annuloplasty rings on anterior mitral leaflet strains in healthy, beating ovine hearts. We tested the hypothesis that rigid, complete rings with non-physiological 3-D shapes, but not saddle-shaped rigid rings or flexible partial bands, increase maximum principal strains across the anterior mitral leaflet.

METHODS

All animals received humane care in compliance with the Principles of Laboratory Animal Care formulated by the National Society for Medical Research and the Guide for Care and Use of Laboratory Animals prepared by the National Academy of Sciences and published by the National Institutes of Health (DHEW [NIH] Publication 85 to 23, revised 1985). This study was approved by the Stanford Medical Center Laboratory Research Animal Review Committee and conducted according to Stanford University policy.

Surgical Preparation

Fifty nine adult, Dorsett-hybrid, male sheep (49±5kg) were premedicated with ketamine (25mg/kg intramuscularly), anesthetized with sodium thiopental (6.8mg/kg intravenously), intubated and mechanically ventilated with inhalational isoflurane (1.0-2.5%). A left thoracotomy was performed and the heart was suspended in a pericardial cradle. Thirteen miniature radiopaque tantalum markers were surgically implanted into the sub-epicardium to silhouette the LV chamber at the intersections of two longitudinal and three crosswise meridians as shown in Figure 1A. Using cardiopulmonary bypass and cardioplegic arrest a total of 33 radiopaque tantalum markers were sewn to the following sites (Figure 1B): 16

around the mitral annulus (17-32, Fig 2A, B), 16 equally spaced on the atrial aspect of the anterior mitral leaflet (AML, 1-16, Fig 2B) and 1 on the central edge of the middle scallop of the posterior mitral leaflet (PML, 33, Fig 2B). A single tantalum loop (0.6mm ID, 1.1mm OD, 3.2 mg) was used for each leaflet marker.

After marker placement, five different annuloplasty ring models, the Cosgrove-Edwards band (COS, Edwards Lifesciences, Irvine, CA, USA, n=12), St. Jude Medical rigid saddle ring (RSAR, St. Jude Medical Inc, St. Paul, MN, USA, n=12), Carpentier-Edwards Physio (PHYSIO, n=12), Edwards IMR ETlogix (ETL, n=11) and Edwards GeoForm (GEO, n=12, all three Edwards Lifesciences, Irvine, CA, USA) were implanted in a releasable fashion as described earlier [8]. In brief, the annuloplasty devices were prepared before the operation in the following manner: The middle parts of eight double-armed polyester braided sutures were stitched evenly spaced around the ring or band from the bottom to the top side using a "spring eye" needle. The resulting loops were "locked" with two polypropylene sutures. The polyester sutures were stitched equidistantly in a perpendicular direction from the ventricular to the atrial side through the mitral annulus. The annuloplasty devices were secured to the mitral annulus by tying these sutures. The "locking sutures" (polypropylene) and the drawstrings were exteriorized before closing the atrium. Ring and band sizes were determined by assessing the entire area of the anterior mitral leaflet using a sizer from Edwards Lifesciences. All annuloplasty devices were true-sized (as all animals had similarly sized leaflets, each received size 28 rings or bands). The left atrium (LA) was closed and the left circumflex artery (LCx) was encircled with a vessel loop for a parallel study [9]. Data from mitral annular and leaflet geometry using this dataset have been published earlier [8-11]. The animals were then transferred to the experimental catheterization laboratory for data acquisition under acute open-chest conditions.

Data Acquisition

Videofluoroscopic images (60 frames/sec) of all radiopaque markers were acquired using biplane videofluoroscopy (Philips Medical Systems, North America, Pleasanton, CA, USA). First, images were acquired under baseline conditions with the ring inserted (COS, RSAR, PHYSIO, ETL, GEO). Following the data acquisition under baseline conditions, 90sec of ischemia were induced, for a parallel study, by tightening the encircling LCx vessel loop with a tourniquet. Thereafter, the "locking sutures" were pulled out and the ring was lifted away from the mitral annulus towards the left atrial roof using the drawstrings. After hemodynamic values returned to baseline, a third data acquisition was performed and images were acquired under baseline conditions with the ring released (COS-CTRL, RSAR-CTRL, PHYSIO-CTRL, ETL-CTRL, GEO-CTRL). Marker coordinates from two consecutive sinus rhythm heart beats from each of the biplane views were then digitized and merged to yield the 3-D coordinates of each marker centroid in each frame using semi-automated image processing and digitization software [12]. Simultaneously, analog left ventricular pressures (LVP) as well as electrocardiogram (ECG) signals were recorded in real-time on the video images during data acquisition.

Hemodynamic Parameters and Cardiac Cycle Timing

For each beat, the end-diastolic videofluoroscopic frame was defined as the frame that coincided with the peak of the R-wave on the ECG. In order to calculate leaflet strains, a reference configuration during diastole and a deformed configuration during peak systole were determined for each beat (t_0 and t_n, respectively, Figure 2). When defining these configurations the goal was to quantify strains with the mitral valve closed in both configurations and maximize the LVP difference between the two time points. To identify the reference configuration, the distance between AML central edge (#4, Figure 1B) and PML edge marker (#33, Figure 1B) was plotted throughout the cardiac cycle for each animal. For each heartbeat the time point of leaflet opening was defined as the time point immediately before the AML and PML started to separate (Figure 2), thereby defining the reference state for beat 1 (t_{01}, Figure 2) and beat 2 (t_{02}, Figure 2). To identify the deformed configuration, LVP curves were plotted throughout the cardiac cycle. The time point of maximum LVP for each heartbeat was defined as the deformed state (t_{n1} and t_{n2}, respectively, Figure 2). The embedded period between these two states closely reflects the period of isovolumetric relaxation (IVR, Figure 2). Maximum systolic dP/dt (dP/dt_{max}) was calculated for each beat for each animal. LV volumes (LVV) were calculated from space-filling tetrahedral fit between all LV markers at each beat at end-diastole (LVEDV), t_{n1}, t_{n2}, t_{01} and t_{02} (See Ref [13] for details). Changes in LVP and LVV (Δ_{LVP} and Δ_{LVV}, respectively) from t_{01} to t_{n1} and from t_{02} to t_{n2} were calculated as $LVPt_{n1} - LVPt_{01}$, $LVPt_{n2} - LVPt_{02}$, and $LVVt_{n1} - LVVt_{01}$, $LVVt_{n2} - LVVt_{02}$,respectively.

Mitral Annular Dimensions

At t_{n1}, t_{n2}, t_{01} and t_{02} distances between markers #20 and #28 and those between #32 and #24 (Figure 1B) were calculated to determine septal-lateral (S-L) and commissure-commissure (C-C) annular dimensions, respectively. Changes in mitral annular S-L and C-C dimensions ($\Delta_{S\text{-}L}$ and $\Delta_{C\text{-}C}$, respectively) from t_{01} to t_{n1} and from t_{02} to t_{n2} were calculated as $t_{n1} - t_{01}$ and $t_{n2} - t_{02}$.

Global Maximum Principal (global ε_{max}), Radial (global ε_{rad}) and Circumferential (global ε_{cir}) Strains

In order to determine the largest (global) maximum principal, radial and circumferential strains across the entire leaflet, the 16 AML mitral leaflet markers (#1-#16, Figure 1B) and the seven mitral annular markers (#17-#23, Figure 1B) were triangulated and 30 triangular membrane elements were generated. For each triangle, the co- and contravariant base vectors at time points t_{01}, t_{n1}, t_{02}, and t_{n2}, were calculated to determine the corresponding metric tensors and the resulting Euler-Almansi strain tensors for beats 1 and 2. The direction defined by the belly markers #9 and 11# (Figure 1B) in the deformed configuration, i.e., at times t_{n1} and t_{n2} for beat 1 and beat 2, respectively, was interpreted as the circumferential direction. The radial direction was defined orthogonal to the circumferential axis, passing through belly marker #10 (see Fig 1B). The largest projections of the Euler-Almansi strain tensor onto the circumferential and radial directions were defined as global maximum circumferential strain (global ε_{cir}) and global maximum radial strain (global ε_{rad}), respectively. These values were determined for two beats in each animal, and each state (with and without annuloplasty device implanted). The animal global maximum principal strain (global ε_{max}) was calculated as the two-beat average for each animal and each state by solving the eigenvalue problem for the Euler-Almansi strain tensor.

Maximum Principal (ε_{max},), Radial (ε_{rad}) and Circumferential (ε_{cir}) Strains Across the Entire Anterior Mitral Leaflet

In order to provide a qualitative description of changes in strain patterns across the entire AML with and without annuloplasty device implanted, the two-beat averages of ε_{max}, ε_{rad} and ε_{cir} values of each triangular element were calculated for each animal in each state. These values were averaged for all animals (by extrapolating constant average element strains to the individual marker positions using super-convergent patch recovery to obtain smoothly varying strain profiles) and plotted onto color mapped schematics.

Statistical Analysis

Average values of all animals in the respective groups were reported as mean ± 1 SD. All data reported for individual animals and all data used for quantitative statistical comparisons are two beat averages. Data with and without annuloplasty ring (or band) were compared using 1-way repeated-measures analysis of variance with a Holm–Sidak post hoc test (Sigmaplot 11.0, Systat Software Inc). To look at strain differences between the ring groups, maximum principal (ε_{max},), radial (ε_{rad}) and circumferential (ε_{cir}) strains with rings (COS, RSAR, PHYSIO, ETL and GEO) were compared using 1-way analysis of variance. A *P* value of less than .05 was considered statistically significant.

RESULTS

Heart rate, LVEDV and dP/dt$_{max}$

Group mean heart rates, LVEDVs and dP/dt$_{max}$ are shown in Table 1. No significant differences were found between ring and Control states in all five groups (except for Cosgrove, where dP/dt$_{max}$ was slightly higher compared to Control).

LV Pressures and Volumes at Reference State (t_0) and Deformed State (t_n)

Table 2 shows LVPs and LVVs at t_0 and t_n as well as Δ_{LVP} and Δ_{LVV}. Δ_{LVP} and Δ_{LVV} are also graphically depicted in Figure 3 (top row). A significant increase in LVPs by approximately 80mmHg (note that changes in LVP and LVV (Δ_{LVP} and Δ_{LVV}) are described from t_0 to t_n, i.e. backward in time) occurred in both ring and Control states from t_0 to t_n, while no relevant LVV changes were observed.

Mitral Annular Dimensions at Reference State (t_0) and Deformed State (t_n)

Table 3 shows the mitral annular S-L and C-C dimensions at t_n and t_0 as well as $\Delta_{S\text{-}L}$ and $\Delta_{C\text{-}C}$. $\Delta_{S\text{-}L}$ and $\Delta_{C\text{-}C}$ are also graphically depicted in Figure 3 (middle row). Again, please note that $\Delta_{S\text{-}L}$ and $\Delta_{C\text{-}C}$ are described from t_0 to t_n, i.e. backward in time. Consequently, negative $\Delta_{S\text{-}L}$ and $\Delta_{C\text{-}C}$ represent an increase, whereas positive $\Delta_{S\text{-}L}$ and $\Delta_{C\text{-}C}$ represent a decrease in the respective dimension during the regular cardiac cycle. Relative to Control, implantation of either complete, rigid rings (RSAR, PHYSIO, ETL or GEO) or the flexible band (COS) resulted in significantly smaller mitral annular S-L and C-C dimensions. Decreases in S-L and C-C diameters from t_0 to t_n (negative $\Delta_{S\text{-}L}$ and $\Delta_{C\text{-}C}$, Table 3) were observed for the Control cases (all groups). With the annuloplasty device implanted, the S-L dimension became slightly smaller from t_0 to t_n with COS ($\Delta_{S\text{-}L}$: −0.9±0.5mm, Table 3 and Figure3, middle row) while no relevant decreases in S-L and C-C diameters from t_0 to t_n were found with RSAR, PHYSIO, ETL or GEO.

Global Maximum Principal (global ε_{max}), Radial (global ε_{rad}) and Circumferential (global ε_{cir}) Strains

Table 4 shows global ε_{max}, ε_{rad} and ε_{cir} for all five groups with and without annuloplasty devices implanted. Global ε_{max}, ε_{rad} and ε_{cir} (average from all animals) are also graphically displayed in Figure 3 (bottom row). Compared to the respective Control state, strains increased significantly with RSAR, PHYSIO, ETL and GEO (0.14±0.05 *vs.* 0.16±0.05, p=0.024, 0.15±0.03 *vs.* 0.18±0.04, p=0.020, 0.11±0.05 *vs.* 0.14±0.05, p=0.042 and 0.13±0.05 *vs.* 0.16±0.05, p=0.009, respectively, all p<0.05), but not with COS (0.15±0.05 vs. 0.15±0.04, n.s., p=0.973). Global ε_{rad} increased significantly compared to the Control state only with RSAR, while greater global ε_{cir} values were found with RSAR, PHYSIO, ETL and GEO (however, insignificant for GEO, Table 4). No significant changes in global ε_{rad} or ε_{cir} were found with COS compared to the Control state. With no annuloplasty device implanted, global ε_{rad} was greater than global ε_{cir} in all five groups (COS-CTRL, RSAR-CTRL, PHYSIO-CTRL, ETL-CTRL, GEO-CTRL, Table 4 and Figure 3, bottom row). With annuloplasty device implanted, global ε_{rad} values were either greater than global ε_{cir} (COS, RSAR), smaller (PHYSIO) or similar (ETL, GEO, Table 4 and Figure 3, bottom row). No differences in ε_{max} (p=0.331, F=1.178), ε_{rad} (p=0.188, F=1.598) or ε_{cir} (p=0.160, F=1.716) with rings implanted were found between the groups (COS, RSAR, PHYSIO, ETL and GEO).

Maximum Principal (ε_{max}), Radial (ε_{rad}) and Circumferential (ε_{cir}) Strains Across the Entire Anterior Mitral Leaflet

Figure 4 shows ε_{max}, ε_{rad} and ε_{cir} across the entire AML for both states, with and without annuloplasty device implanted in all five groups. Increases in ε_{max} can be appreciated with RSAR, PHYSIO, ETL and GEO compared to the respective Control state and predominantly occur in the belly and edge region of the anterior mitral leaflet. No major changes in strain patterns (ε_{max}, ε_{rad} or ε_{cir}) were observed with COS. ε_{max} values across the AML of the respective Control states were slightly different between groups with COS-CTRL, RSAR-CTRL and PHYSIO-CTRL being more strained than GEO-CTRL and ETL-CTRL.

DISCUSSION

The principle finding of this study was that, with no relevant changes in hemodynamics, implantation of rigid, complete annuloplasty rings (RSAR, PHYSIO, ETL and GEO), but not of the flexible partial band (COS), increased global maximum principal strains of the AML. These changes predominantly occurred in the region of the AML belly and edge.

Several studies have determined mitral leaflet strains and stretches using a variety of different techniques [4-7, 14-19]. *In vitro* studies have been employed to characterize dynamic stretches on the anterior and posterior leaflet of excised porcine mitral valves using a left heart simulator [6, 14-17]. *In vivo* studies, using sonomicrometer technology, quantified AML strains in the beating ovine heart [16] and lastly, finite element studies investigated strain patterns across the AML [4, 5, 18, 19].

Salgo et al. demonstrated in a numerical simulation that the native mitral annular shape is important to minimize stresses acting on the leaflet [5]. In a previous analysis from the same dataset we demonstrated that implantation of the Physio, IMR ETLogix and GeoForm, but not RSAR, perturbed the physiological saddle-shape of the mitral annulus [11]. The increased maximum principal leaflet strains observed with these three rings are therefore consistent with engineering intuition quantified through the results of Salgo et al.. However, to our surprise, the supposedly physiologically shaped RSAR also led to an increase in maximum principal leaflet strains. Assuming that the shape of this ring is physiological it could be speculated that the dynamic motion of the mitral annulus rather than its 3-D shape is of major importance to preserve AML strain distribution. This hypothesis, however, is contrary to previous studies that suggested changes in the physiological mitral annular 3-D saddle shape lead to increases in leaflet strains [6]. It may therefore also be speculated that the shape of the RSAR does not fully represent the natural 3-D annular shape and that, as discussed earlier [6], increased strains are also a result of a non-physiological annular shape.

The partial, flexible band (COS) has been found to preserve the mitral annular saddle shape [11] and allow minimal mitral annular S-L dynamics (Figure 3, middle row) during the observed time period (from t_0 to t_n). However, COS significantly reduced mitral annular dimensions compared to the Controlstate (Table 3 and Ref [11]). Since COS did not affect AML strains (Figure 3, bottom row) we speculate that preserving physiologic mitral annular dynamics and shape rather than absolute mitral annular dimensions are the key components to maintaining a physiological strain distribution across the AML.

To our knowledge, Votta et al. were the only group that quantified the effects of annuloplasty rings (GeoForm and Physio) on mitral leaflet strains and stresses [4]. The group used a finite element model and demonstrated that the GeoForm, but not the Physio, reduced maximum principal mitral leaflet stresses during simulated functional mitral regurgitation [4]. In our study we found that all rigid rings (RSAR, PHYSIO, ETL and GEO) increased maximum principal AML strains, irrespective of their 3-D shape. However, unlike Votta et al., we used an *in vivo* model of the normal, beating heart. We therefore cannot comment on the potential effects of FMR/IMR rings in the diseased state and it is possible that these rings restore a physiological strain distribution in hearts with dilated LVs.

In our study we report the effect of different annuloplasty devices on radial and circumferential strains. While global ε_{rad} was only greater with RSAR, global ε_{cir} was greater with all rigid, complete rings (RSAR, PHYSIO, ETL and GEO, Table 4) compared to the Control state (however, insignificantly for GEO), suggesting that rigid, complete annuloplasty devices affect circumferential strains more than radial strains. The reason for the insignificant increase in global ε_{cir} observed with GEO could be a result of the larger commissure to commissure dimension of this ring compared to RSAR, PHYSIO or ETL [3], suggesting that the physiological circumferential AML strain distribution is sensitive to the amount of mitral annular C-C decrease.

Study Limitations

Several limitations should be addressed to allow a better interpretation of these data. First, the data were acquired from open-chest, anesthetized ovine hearts with normal preoperative anatomy. Considerable caution must therefore be exercised when extrapolating these findings to the human heart. This is especially true for the GeoForm and IMR ETLogix rings that have been designed for patients with IMR/FMR (with distorted annular, leaflet and ventricular geometry and function). As mentioned above, if these rings are implanted in the setting of FMR/IMR, it could well be that they reduce (or restore physiological) leaflet strains as demonstrated by Votta and colleagues in a computer simulation [4]. In future analyses we aim to use our experimental *in vivo* data to determine whether these two FMR/IMR-specific rings (GEO and ETL) are more efficient than conventional rings in terms of reducing leaflet strains during acute myocardial ischemia. Second, AML strains were quantified for only the IVR phase of the cardiac cycle and it could be that the rings affect strain patterns differently in other phases of the cardiac cycle [20]. Third, although perturbed leaflet strains have been associated with impaired mitral valve repair durability [6, 7] currently no study exists that proves causation. Consequently, it remains to be determined whether perturbations in AML strains impair long-term function of the mitral valve after repair. Fourth, when radial and circumferential strains were plotted onto color mapped schematics (Figure 4), we did not only observe tensile, but also compressive strains in both Control states and with rings implanted (green and blue areas, Figure 4). Compressive strains do not occur, *e.g*., in purely computational models that use simplified AML shapes with the leaflet being entirely convex to the left ventricle [4] and, thus, may be a result of the complex AML shape [21] that was included in our analyses. The finding of compressive strains warrants further investigation; however, we focused on the tensile aspects of strain in this manuscript and did not perform detailed analyses of compressive strain patterns. Fifth, no statistically significant differences in strains were found between the different ring types. We therefore cannot draw any conclusions from these data whether one ring design is superior to another; however, this study was not adequately powered to demonstrate differences between the different ring types. Sixth, we only studied a partial, flexible band. Since no complete, flexible ring was examined in this experiment it is not possible to distinguish whether the observed lack of increase in AML strains with a partial band is due to its partial design, its flexibility, or due to a combination of the two. Lastly, strain patterns may change with varying annuloplasty device sizes [4]. Since only size 28mm annuloplasty rings were used in this study, we are unable to draw any conclusions about the impact of ring or band size on leaflet strains.

Conclusions

In conclusion, regardless of their three-dimensional shape, rigid, complete annuloplasty rings (RSAR, PHYSIO, ETL, GEO), but not a partial flexible band (COS), increased maximum principal anterior mitral leaflet strains predominantly in the belly and edge regions in the normal beating ovine heart. Large, randomized, clinical trials are needed to answer the question whether the observed ring-induced alterations in mitral leaflet strain states exist in patients, and if so, whether they adversely affect long-term mitral valve repair durability.

Acknowledgments

The authors gratefully acknowledge the expert technical assistance of Paul Chang, Maggie Brophy, Sigurd Hartnett, Erin Schultz and George T. Daughters as well as the inspiring suggestions of Frank Langer.

FUNDING SOURCES D. Craig Miller, M.D.: R01 research grant, NHLBI, National Institutes of Health HL29589 (1982-2008), R01 research grant, NHLBI, National Institutes of Health HL67025 (2001-2010) Wolfgang Bothe, M.D.: Research Grant S/06/07, Deutsche Herzstiftung, Frankfurt, Germany Ellen Kuhl, Ph.D.: NSF CAREER Award CMMI-0952021

John-Peder Escobar Kvitting, M.D.:U.S.-Norway Fulbright Foundation, the Swedish Heart-Lung Foundation and the Swedish Society for Medical Research.

Julia C. Swanson, M.D.: Western States Affiliate AHA Postdoctoral Fellowship

REFERENCES

1. Ryan LP, Jackson BM, Hamamoto H, Eperjesi TJ, Plappert TJ, St John-Sutton M, Gorman RC, Gorman JH 3rd. The influence of annuloplasty ring geometry on mitral leaflet curvature. Ann Thorac Surg. 2008; 86:749–60. discussion 749-60. [PubMed: 18721556]
2. Accola KD, Scott ML, Thompson PA, Palmer GJ 3rd, Sand ME, Ebra G. Midterm outcomes using the physio ring in mitral valve reconstruction: experience in 492 patients. Ann Thorac Surg. 2005; 79:1276–83. discussion 1276-83. [PubMed: 15797062]
3. Bothe W, Swanson JC, Ingels NB, Miller DC. How much septal-lateral mitral annular reduction do you get with new ischemic/functional mitral regurgitation annuloplasty rings? J Thorac Cardiovasc Surg. 2010; 140:117–21. 121 e1–3. [PubMed: 20074748]
4. Votta E, Maisano F, Bolling SF, Alfieri O, Montevecchi FM, Redaelli A. The Geoform disease-specific annuloplasty system: a finite element study. Ann Thorac Surg. 2007; 84:92–101. [PubMed: 17588392]
5. Salgo IS, Gorman JH 3rd, Gorman RC, Jackson BM, Bowen FW, Plappert T, St John Sutton MG, Edmunds LH Jr. Effect of annular shape on leaflet curvature in reducing mitral leaflet stress. Circulation. 2002; 106:711–7. [PubMed: 12163432]
6. Jimenez JH, Liou SW, Padala M, He Z, Sacks M, Gorman RC, Gorman JH 3rd, Yoganathan AP. A saddle-shaped annulus reduces systolic strain on the central region of the mitral valve anterior leaflet. J Thorac Cardiovasc Surg. 2007; 134:1562–8. [PubMed: 18023684]
7. Padala M, Hutchison RA, Croft LR, Jimenez JH, Gorman RC, Gorman JH 3rd, Sacks MS, Yoganathan AP. Saddle shape of the mitral annulus reduces systolic strains on the P2 segment of the posterior mitral leaflet. Ann Thorac Surg. 2009; 88:1499–504. [PubMed: 19853100]
8. Bothe W, Chang PA, Swanson JC, Itoh A, Arata K, Ingels NB, Miller DC. Releasable annuloplasty ring insertion--a novel experimental implantation model. Eur J Cardiothorac Surg. 2009; 36:830–2. [PubMed: 19646892]

9. Bothe W, Kvitting JP, Stephens EH, Swanson JC, Liang DH, Ingels NB Jr. Miller DC. Effects of different annuloplasty ring types on mitral leaflet tenting area during acute myocardial ischemia. J Thorac Cardiovasc Surg. 2011; 141:345–53. [PubMed: 21241857]

10. Bothe W, Kvitting JP, Swanson JC, Goktepe S, Vo KN, Ingels NB, Miller DC. How do annuloplasty rings affect mitral leaflet dynamic motion? Eur J Cardiothorac Surg. 2010; 38:340–9. [PubMed: 20335042]

11. Bothe W, Kvitting JP, Swanson JC, Hartnett S, Ingels NB Jr. Miller DC. Effects of different annuloplasty rings on anterior mitral leaflet dimensions. J Thorac Cardiovasc Surg. 139:1114–22. [PubMed: 20412950]

12. Niczyporuk MA, Miller DC. Automatic tracking and digitization of multiple radiopaque myocardial markers. Comput Biomed Res. 1991; 24:129–42. [PubMed: 2036779]

13. Moon MR, DeAnda A Jr. Daughters GT 2nd, Ingels NB Jr. Miller DC. Experimental evaluation of different chordal preservation methods during mitral valve replacement. Ann Thorac Surg. 1994; 58:931–43. discussion 943-4. [PubMed: 7944814]

14. He Z, Sacks MS, Baijens L, Wanant S, Shah P, Yoganathan AP. Effects of papillary muscle position on in-vitro dynamic strain on the porcine mitral valve. J Heart Valve Dis. 2003; 12:488–94. [PubMed: 12918852]

15. He S, Jimenez J, He Z, Yoganathan AP. Mitral leaflet geometry perturbations with papillary muscle displacement and annular dilatation: an in-vitro study of ischemic mitral regurgitation. J Heart Valve Dis. 2003; 12:300–7. [PubMed: 12803328]

16. Sacks MS, He Z, Baijens L, Wanant S, Shah P, Sugimoto H, Yoganathan AP. Surface strains in the anterior leaflet of the functioning mitral valve. Ann Biomed Eng. 2002; 30:1281–90. [PubMed: 12540204]

17. Jimenez JH, Soerensen DD, He Z, He S, Yoganathan AP. Effects of a saddle shaped annulus on mitral valve function and chordal force distribution: an in vitro study. Ann Biomed Eng. 2003; 31:1171–81. [PubMed: 14649491]

18. Kunzelman KS, Reimink MS, Cochran RP. Annular dilatation increases stress in the mitral valve and delays coaptation: a finite element computer model. Cardiovasc Surg. 1997; 5:427–34. [PubMed: 9350801]

19. Votta E, Maisano F, Soncini M, Redaelli A, Montevecchi FM, Alfieri O. 3-D computational analysis of the stress distribution on the leaflets after edge-to-edge repair of mitral regurgitation. J Heart Valve Dis. 2002; 11:810–22. [PubMed: 12479282]

20. Itoh A, Krishnamurthy G, Swanson JC, Ennis DB, Bothe W, Kuhl E, Karlsson M, Davis LR, Miller DC, Ingels NB Jr. Active stiffening of mitral valve leaflets in the beating heart. Am J Physiol Heart Circ Physiol. 2009; 296:H1766–73. [PubMed: 19363135]

21. Ryan LP, Jackson BM, Eperjesi TJ, Plappert TJ, St John-Sutton M, Gorman RC, Gorman JH 3rd. A methodology for assessing human mitral leaflet curvature using real-time 3-dimensional echocardiography. J Thorac Cardiovasc Surg. 2008; 136:726–34. [PubMed: 18805278]

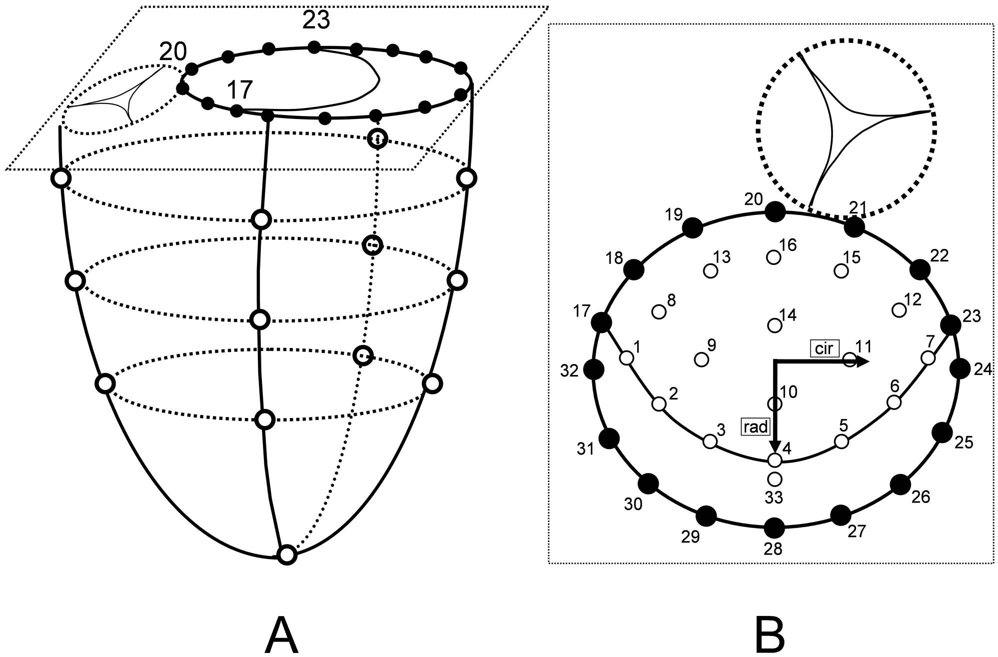

Fig 1.

A: Schematic illustrating ventricular and annular marker locations. Marker #20 represents the mitral annular saddle horn marker and markers #17 and #23 the anterior and posterior commissural markers, respectively. **B**: Schematic magnification of a top view of the mitral valve showing annular as well as leaflet markers. Sixteen markers were placed on the mitral annulus (#17-#32), 16 markers were placed on the anterior mitral leaflet (#1-#16) and one marker was placed on the free edge of the mid part of the posterior leaflet (#33). Inset shows the radial (rad) and circumferential (cir) directions used for strain definitions.

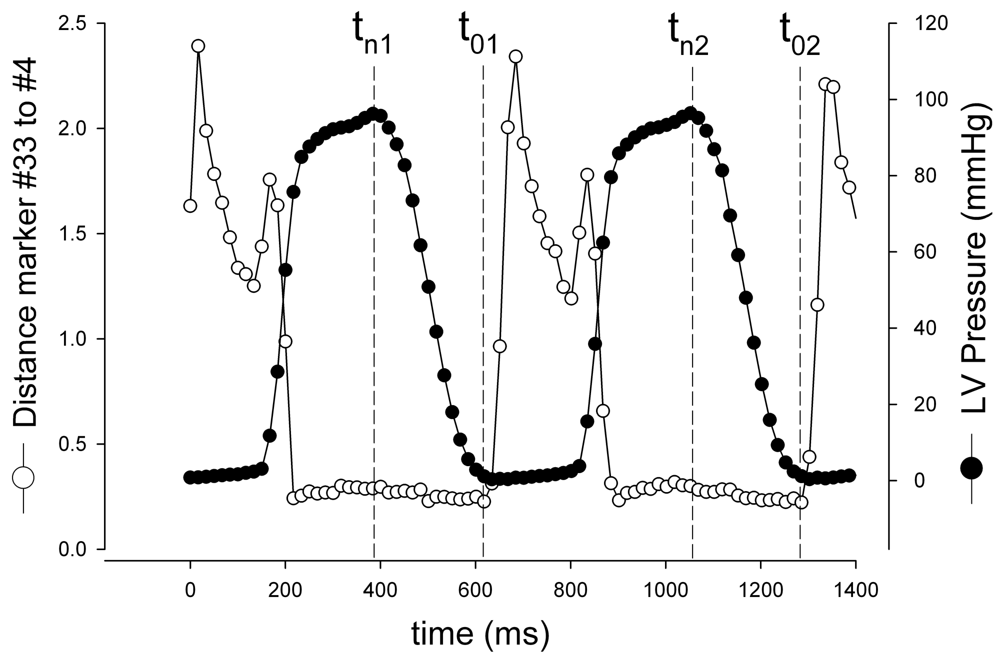

Fig 2.

Illustration of time point definitions. Time point t_n (strained state) was defined as maximum LV pressure for beat 1 (t_{n1}) and beat 2 (t_{n2}). Time point t_0 (reference state) was defined as last time frame before mitral leaflet separation (as represented by the rapid increase in plotted curve of distances (cm) between marker #33 and #4, see Fig 1) for beat 1 (t_{01}) and beat 2 (t_{02}).

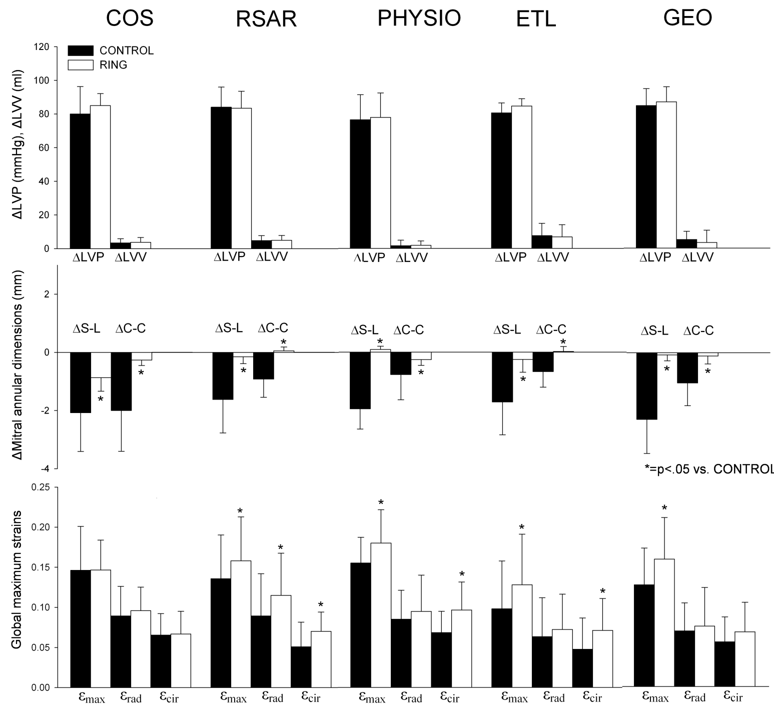

Fig 3.

Changes in LV pressure and volumes (ΔLVP and ΔLVV, respectively (top row), mitral annular dimensions (middle row) from reference state (t_0) to strained state (t_n) as well as global maximum principal (ε_{max}), radial (ε_{rad}) and circumferential (ε_{cir}) (bottom row). Note that changes from t_0 to t_n include a calculation from a time point later in the cardiac cycle (t_0) to an earlier time point of the cardiac cycle (t_n). COS=Edwards Cosgrove band, RSAR=St Jude Medical rigid saddle-shaped annuloplasty ring, ETL=Edwards IMR ETlogix, GEO=Edwards GeoForm. Values are mean±1SD.

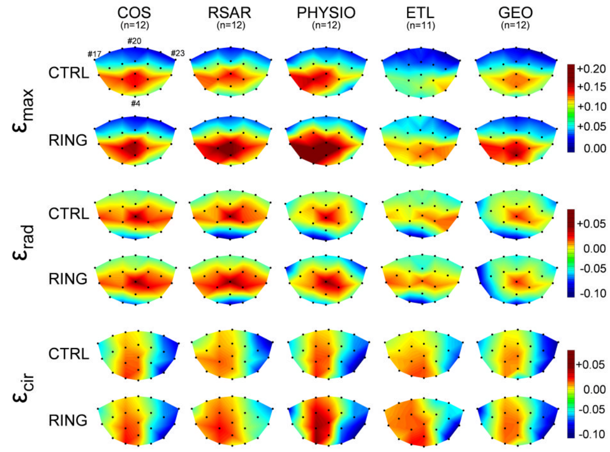

Fig 4.

Color-mapped schematics of maximum principal (ε_{max}, two top rows), radial (ε_{rad}, two middle rows) and circumferential (ε_{cir}, two bottom rows) strains across the entire anterior mitral leaflet for the Control state (CTRL) and with annuloplasty device implanted (RING). Markers #17 and #23 depict anterior and posterior commissures, respectively, marker #20 represents the mid-septal mitral annulus (saddle horn, see Figure 1). COS=Edwards Cosgrove band, RSAR=St Jude Medical rigid saddle-shaped annuloplasty ring, ETL=Edwards IMR ETlogix, GEO=Edwards GeoForm.

TABLE 1

Heart rate (HR), LV end-diastolic volume (LVEDV) and dP/dt_{max}

		Animal no												Mean±1SD					
		1	**2**	**3**	**4**	**5**	**6**	**7**	**8**	**9**	**10**	**11**	**12**	**HR (min^{-1})**	**P vs. CTRL**	**LVEDV (ml)**	**P vs. CTRL**	**dP/dt_{max} (mmHg)**	**P vs. CTRL**
	HR (min^{-1})	89	104	124	103	87	76	114	90	100	113	85	94	98±14					
COS-CTRL	LVEDV (ml)	109	104	107	137	136	111	132	100	113	122	149	122			120±15			
	dP/dt_{max} (mmHg)	979	1619	1289	1069	1853	1514	1742	1238	1478	1564	846	1128					1360±317	
	HR (min^{-1})	97	111	118	101	87	73	114	90	97	111	86	94	98±13	.914				
COS	LVEDV (ml)	109	100	118	139	137	117	132	100	111	122	149	119			121±16	.392		
	dP/dt_{max} (mmHg)	1280	1905	1309	1100	2018	1635	2196	1294	1739	1636	970	1240					1527±386	.001
	HR (min^{-1})	74	122	113	94	71	88	88	86	106	66	87	77	89±17					
RSAR-CTRL	LVEDV (ml)	91	80	135	100	122	112	140	156	113	136	123	138			121±22			
	dP/dt_{max} (mmHg)	1309	2296	1267	1109	1055	1794	1082	1381	1039	1232	708	1125					1283±409	
	HR (min^{-1})	77	113	114	96	73	90	89	85	104	67	85	74	89±15	.853				
RSAR	LVEDV (ml)	96	85	139	103	124	110	138	149	111	133	123	140			121±20	.714		
	dP/dt_{max} (mmHg)	1202	1817	1313	1312	1145	1692	1131	1011	1087	1111	682	1212					1226±297	.340
	HR (min^{-1})	84	118	107	80	99	84	88	82	88	100	87	90	92±12					
PHYSIO-CTRL	LVEDV (ml)	174	136	112	136	126	87	124	119	99	126	120	128			124±21			
	dP/dt_{max} (mmHg)	1694	1187	1307	841	1343	1551	1014	1116	1948	1239	888	1560					1307±333	
	HR (min^{-1})	84	111	107	78	103	83	88	82	91	99	88	88	92±11	.517				
PHYSIO	LVEDV (ml)	178	138	118	139	116	80	125	118	96	128	123	128			124±24	.934		
	dP/dt_{max} (mmHg)	1896	1186	1290	835	1683	1757	1166	1056	1426	1362	913	1606					1348±337	.523
ETL-CTRL	HR (min^{-1})	87	79	85	76	76	79	78	80	91	94	74		82±6					

		Animal no												Mean±1SD					
		1	**2**	**3**	**4**	**5**	**6**	**7**	**8**	**9**	**10**	**11**	**12**	**HR (min^{-1})**	**P vs. CTRL**	**LVEDV (ml)**	**P vs. CTRL**	**dP/dt_{max} (mmHg)**	**P vs. CTRL**
	LVEDV (ml)	145	105	96	147	115	94	120	140	125	148	139				125±20			
	dP/dt_{max} (mmHg)	1879	681	1630	1064	1091	1348	1085	821	728	1322	1207						1169±368	
	HR (min^{-1})	60	79	83	81	75	80	78	83	91	96	74		80±9	.531				
ETL	LVEDV (ml)	150	104	96	147	120	98	117	139	123	145	137				125±20	.833		
	dP/dt_{max} (mmHg)	1860	686	1591	1053	1098	1399	1073	874	772	1492	1188						1190±363	.259
	HR (min^{-1})	80	82	94	100	96	106	106	86	85	106	84	82	92±10					
GEO-CTRL	LVEDV (ml)	89	113	120	114	122	131	131	107	113	95	109	130			114±13			
	dP/dt_{max} (mmHg)	1030	1238	1298	1248	1469	1043	1163	1392	1138	1342	2221	1180					1313±315	
	HR (min^{-1})	83	79	95	103	97	104	109	91	99	96	84	79	93±10	.492				
GEO	LVEDV (ml)	89	116	119	105	119	130	129	101	107	104	106	129			113±13	.223		
	dP/dt_{max} (mmHg)	1070	1259	1398	1144	1569	1181	1372	1509	1110	1321	2586	1131					1388±41	.070

All values from individual animals are two beat averages, COS=Edwards Cosgrove band, RSAR=St Jude Medical rigid saddle-shaped annuloplasty ring, ETL= Edwards IMR ETlogix, GEO=Edwards GeoForm, SD=standard deviation

TABLE 2

Left ventricular pressures and volumes at reference state (t0) and strained state (tn)

			Animal no												Mean±1SD											
															LVP (mmHg)						LVV (ml)					
			1	2	3	4	5	6	7	8	9	10	11	12	t0	P vs. CTRL	tn	P vs. CTRL	Δtn-t0	P vs. CTRL	t0	P vs. CTRL	tn	P vs. CTRL	Δtn-t0	P vs. CTRL
		t_0	20	10	45	17	24	12	15	9	7	6	18	7	16±11											
	LVP (mmHg)	t_n	87	97	82	105	109	100	95	87	103	94	88	103			96±8									
COS-CTRL		Δ_{tn-t0}	68	88	37	89	85	88	79	78	96	88	69	96					80±16							
		t_0	87	78	88	122	94	81	86	72	91	102	108	99							92±14					
	LVV (ml)	t_n	91	85	89	124	97	82	92	80	92	101	112	102									96±13			
		Δ_{tn-t0}	4.1	6.7	1.1	1.6	3.7	1.8	6.1	7.6	0.9	−0.6	4.0	3.0											3.3±2.5	
		t_0	13	10	18	17	24	17	15	10	5	2	12	6	12±6	.188										
	LVP (mmHg)	t_n	90	99	90	100	109	107	98	91	100	97	92	97			97±6	.218								
COS		Δ_{tn-t0}	77	89	71	84	85	90	83	81	94	95	81	91					85±7	.132						
		t_0	90	76	101	126	89	81	80	72	87	101	109	97							92±15	.940				
	LVV (ml)	t_n	93	81	102	126	94	85	88	80	88	101	116	99									96±14	.708		
		Δ_{tn-t0}	3.6	5.6	0.8	0.6	4.4	3.9	8.0	7.6	0.9	−0.1	7.3	2.2											3.7±2.9	.323
		t_0	39	4	12	21	11	15	25	19	14	7	17	14	16±9											
	LVP (mmHg)	t_n	100	96	101	91	97	125	107	107	95	98	95	96			101±9									
RSAR - CTRL		Δ_{tn-t0}	61	92	89	71	86	109	82	87	80	91	78	82					84±12							
		t_0	75	63	113	77	83	81	109	113	90	102	103	101							92±17					
	LVV (ml)	t_n	74	68	120	79	93	89	113	117	94	108	106	106									97±17			
		Δ_{tn-t0}	−1.1	5.7	6.6	1.7	10.3	8.4	3.5	3.7	4.3	6.2	2.9	4.6											4.7±3.0	

			Animal no												Mean±1SD											
															LVP (mmHg)						LVV (ml)					
			1	2	3	4	5	6	7	8	9	10	11	12	t0	P vs. CTRL	tn	P vs. CTRL	Δtn-t0	P vs. CTRL	t0	P vs. CTRL	tn	P vs. CTRL	Δtn-t0	P vs. CTRL
RSAR	LVP (mmHg)	t_0	33	7	10	21	10	13	18	18	13	7	8	11	14±7	.040										
		t_n	92	91	102	95	102	109	95	101	95	97	94	98			98±5	.144								
		$\Delta_{tn\text{-}t0}$	59	83	92	75	92	96	77	82	83	90	86	87					83±10	.752						
	LVV (ml)	t_0	75	67	120	81	85	81	110	115	88	102	102	103							94±17	.027				
		t_n	75	75	124	83	95	89	114	121	92	107	107	107									99±17	.022		
		$\Delta_{tn\text{-}t0}$	−0.2	7.9	4.1	2.4	10.7	7.5	3.5	6.0	4.0	4.8	5.4	3.5											5.0±2.9	.639
PHYSIO-CTRL	LVP (mmHg)	t_0	32	2	24	6	13	41	33	5	2	37	10	12	18±14											
		t_n	95	81	85	83	108	97	95	96	101	101	95	97			95±8									
		$\Delta_{tn\text{-}t0}$	63	79	61	77	95	56	62	91	99	64	85	85					76±15							
	LVV (ml)	t_0	123	102	94	113	96	72	88	95	66	105	93	97							95±16					
		t_n	122	109	94	116	98	69	88	100	70	100	95	102									97±16			
		$\Delta_{tn\text{-}t0}$	−1.1	6.4	−0.1	2.7	1.5	−2.2	−0.1	5.6	4.1	−4.5	2.2	4.4											1.6±3.3	
PHYSIO	LVP (mmHg)	t_0	28	2	26	4	7	46	29	3	2	33	11	8	17±15	.124										
		t_n	97	83	86	87	103	98	97	96	95	99	99	97			95±6	.949								
		$\Delta_{tn\text{-}t0}$	69	81	60	83	96	52	67	93	92	65	89	89					78±15	.221						
	LVV (ml)	t_0	123	107	97	119	95	62	87	98	71	105	97	99							97±17	.285				
		t_n	123	112	100	122	95	61	87	100	75	102	101	103									98±18	.236		
		$\Delta_{tn\text{-}t0}$	−0.6	5.8	3.4	3.4	0.4	−1.6	0.4	1.9	4.1	−2.8	3.4	3.8											1.8±2.6	.657
ETL-CTRL	LVP (mmHg)	t_0	10	19	10	15	17	13	15	11	14	11	21		14±4											
		t_n	95	93	98	92	90	89	105	91	91	98	103				95±5									

			Animal no												Mean±1SD											
															LVP (mmHg)						LVV (ml)					
			1	2	3	4	5	6	7	8	9	10	11	12	t0	P vs. CTRL	tn	P vs. CTRL	Δtn-t0	P vs. CTRL	t0	P vs. CTRL	tn	P vs. CTRL	Δtn-t0	P vs. CTRL
		Δ_{tn-t0}	85	74	88	77	73	75	89	80	77	86	81						81±6							
		t_0	96	87	64	110	87	68	90	104	104	107	110								93±16					
	LVV (ml)	t_n	123	89	77	115	95	70	91	112	105	115	120										101±18			
		Δ_{tn-t0}	26.9	2.1	12.3	5.6	8.0	2.9	0.9	7.5	0.7	7.1	9.2												7.6±7.4	
		t_0	11	11	8	9	13	12	13	10	12	12	15		11±2	.010										
	LVP (mmHg)	t_n	98	93	103	90	93	94	101	95	94	98	98				96±4	.306								
ETL		Δ_{tn-t0}	87	82	95	80	79	82	88	85	83	87	83						85±4	.080						
		t_0	97	91	66	114	93	72	89	106	107	104	115								96±16	.015				
	LVV (ml)	t_n	123	94	77	115	101	74	91	114	106	113	122										103±17	.034		
		Δ_{tn-t0}	25.2	2.7	11.0	1.6	7.7	2.2	1.8	8.1	−1.2	9.1	6.8												6.8±7.2	.186
		t_0	18	13	33	16	17	8	11	1	3	3	3	15	12±9											
	LVP (mmHg)	t_n	98	91	100	111	105	105	86	96	96	88	93	88			96±8									
GEO-CTRL		Δ_{tn-t0}	81	77	67	95	88	98	75	95	93	85	90	72					85±10							
		t_0	70	74	99	86	102	118	99	84	88	75	81	90							89±14					
	LVV (ml)	t_n	77	88	103	93	99	125	101	92	90	74	85	99									94±14			
		Δ_{tn-t0}	7.0	14.0	4.1	7.7	−3.9	7.8	2.3	7.8	2.4	−1.0	3.6	9.0											5.1±4.8	
		t_0	17	10	24	15	14	8	8	1	2	7	6	8	10±6	.175										
	LVP (mmHg)	t_n	93	90	96	110	101	111	92	96	99	92	96	88			97±7	.589								
GEO		Δ_{tn-t0}	76	81	73	95	87	103	83	95	97	85	90	81					87±9	.088						
	LVV (ml)	t_0	74	77	102	86	98	122	98	83	91	92	82	91							91±13	.131				

	Animal no												Mean±1SD											
													LVP (mmHg)						LVV (ml)					
	1	2	3	4	5	6	7	8	9	10	11	12	t0	P vs. CTRL	tn	P vs. CTRL	Δtn-t0	P vs. CTRL	t0	P vs. CTRL	tn	P vs. CTRL	Δtn-t0	P vs. CTRL
t_n	78	92	105	92	97	130	101	90	91	78	82	102									95±14	.289		
$\Delta_{tn\text{-}t0}$	4.0	14.6	2.6	6.1	−1.6	7.9	2.5	7.0	0.6	−14.7	0.7	10.6											3.4±7.3	.175

All values from individual animals are two beat averages, t_n=strained state (time point of maximum LVP), t_0=reference strain state (time point before mitral valve opening, see METHODS), COS=Edwards Cosgrove band, RSAR=St Jude Medical rigid saddle-shaped annuloplasty ring, ETL= Edwards IMR ETlogix, GEO=Edwards GeoForm, SD=standard deviation

TABLE 3

Mitral annular septal-lateral (S-L) and commissure-commissure (C-C) dimensions at reference state (t0) and strained state (tn)

			Animal no												Mean±1SD											
															S-L						C-C					
			1	2	3	4	5	6	7	8	9	10	11	12	t0	P vs. CTRL	tn	P vs. CTRL	Δtn-t0	P vs. CTRL	t0	P vs. CTRL	tn	P vs. CTRL	Δtn-t0	P vs. CTRL
COS-CTRL		t_0	29.3	29.9	27.2	33.2	27.2	24.6	32.7	28.8	27.1	25.9	35.7	29.8	29.3±3.3											
	S-L	t_n	27.9	27.4	26.3	28.7	23.0	22.7	30.5	27.5	24.9	26.1	34.6	26.9			27.2±3.2									
		Δ_{tn-t0}	−1.4	−2.4	−1.0	−4.5	−4.2	−1.9	−2.2	−1.3	−2.2	0.2	−1.1	−2.9					−2.1±1.3							
		t_0	36.2	36.9	34.6	37.2	36.9	33.8	40.4	41.6	42.4	36.5	38.9	39.0							37.8±2.7					
	C-C	t_n	35.7	36.2	34.1	36.3	34.1	33.1	39.8	40.6	40.8	35.7	38.0	37.9									36.8±2.6			
		Δ_{tn-t0}	−0.4	−0.7	−0.5	−1.0	−2.8	−0.7	−0.6	−1.0	−1.6	−0.8	−0.9	−1.1											−1.0±0.6	
COS		t_0	23.5	26.1	26.0	29.7	23.9	24.2	30.6	25.9	24.5	26.1	32.2	27.5	26.7±2.8	<.001										
	S-L	t_n	22.9	25.5	25.2	29.1	22.5	22.9	28.9	25.7	23.7	25.5	31.8	26.2			25.8±2.8	.008								
		Δ_{tn-t0}	−0.6	−0.6	−0.9	−0.6	−1.5	−1.3	−1.7	−0.2	−0.7	−0.6	−0.4	−1.3					−0.9±0.5	.006						
		t_0	30.6	32.7	32.0	34.6	32.6	33.6	38.3	38.8	38.0	35.9	35.2	37.9							35.0±2.8	.004				
	C-C	t_n	30.4	32.6	31.7	34.4	32.3	33.4	38.1	38.3	38.1	35.2	34.8	37.6									34.7±2.8	.001		
		Δ_{tn-t0}	−0.3	0.0	−0.3	−0.1	−0.3	−0.2	−0.2	−0.5	0.0	−0.7	−0.4	−0.3											−0.3±0.2	.002
RSAR-CTRL		t_0	30.5	23.3	27.5	27.3	27.6	29.7	29.1	30.8	27.5	33.9	28.5	30.4	28.8±2.6											
	S-L	t_n	30.0	22.9	26.4	27.3	25.9	28.3	27.7	27.1	25.3	30.5	26.6	28.7			27.2±2.1									
		Δ_{tn-t0}	−0.5	−0.3	−1.1	0.0	−1.7	−1.4	−1.4	−3.8	−2.2	−3.5	−1.9	−1.7					−1.6±1.1							
		t_0	37.6	32.7	32.9	35.2	37.7	35.6	36.4	40.1	36.7	42.1	38.6	40.4							37.2±2.9					
	C-C	t_n	36.6	32.5	32.5	34.7	36.3	34.1	35.5	38.0	36.7	41.1	37.3	40.0									36.3±2.7			
		Δ_{tn-t0}	−1.1	−0.2	−0.5	−0.5	−1.4	−1.6	−0.9	−2.2	0.0	−1.0	−1.3	−0.5											−0.9±0.6	
RSAR		t_0	25.4	23.7	24.9	24.1	24.6	25.8	24.8	25.0	23.5	26.5	24.7	24.6	24.8±0.8	<.001										
	S-L	t_n	25.2	24.0	24.6	23.9	24.5	25.7	24.6	24.9	22.9	26.4	24.8	24.4			24.6±0.9	<.001								

			Animal no												Mean±1SD											
															S-L						C-C					
			1	2	3	4	5	6	7	8	9	10	11	12	t0	P vs. CTRL	tn	P vs. CTRL	Δtn-t0	P vs. CTRL	t0	P vs. CTRL	tn	P vs. CTRL	Δtn-t0	P vs. CTRL
		Δ_{tn-t0}	−0.2	0.3	−0.3	−0.3	−0.1	−0.1	−0.2	−0.2	−0.6	−0.1	0.1	−0.2					−0.2±0.2	.001						
		t_0	34.5	33.4	33.7	33.8	33.8	34.6	34.3	33.1	31.1	33.0	31.8	33.8							33.4±1.0	.009				
	C-C	t_n	34.3	33.6	33.7	33.8	33.8	34.5	34.5	33.4	31.3	33.1	31.8	33.9									33.5±1.0	.002		
		Δ_{tn-t0}	−0.2	0.2	0.0	0.0	0.0	−0.1	0.2	0.3	0.1	0.1	−0.1	0.0											0.1±0.1	<.001
PHYSIO-CTRL		t_0	30.1	26.9	26.5	30.5	27.7	25.3	30.5	35.6	27.7	31.2	33.1	30.2	29.6±3.0											
	S-L	t_n	28.6	26.1	24.0	27.6	25.7	24.5	28.4	33.5	25.2	29.6	31.4	27.3			27.7±2.9									
		Δ_{tn-t0}	−1.5	−0.9	−2.4	−2.9	−2.0	−0.8	−2.1	−2.1	−2.5	−1.7	−1.7	−3.0					−2.0±0.7							
		t_0	42.6	37.7	39.0	42.0	40.5	36.7	40.0	43.6	38.9	37.9	40.5	39.6							39.9±2.1					
	C-C	t_n	41.2	39.1	37.5	41.4	39.9	35.7	39.4	43.2	37.1	37.9	39.3	38.4									39.1±2.1			
		Δ_{tn-t0}	−1.4	1.4	−1.6	−0.6	−0.6	−1.1	−0.6	−0.4	−1.9	0.0	−1.2	−1.3											−0.8±0.9	
		t_0	24.2	24.2	24.6	24.1	23.5	23.3	25.0	28.1	24.1	26.1	25.9	26.1	24.9±1.4	<.001										
	S-L	t_n	23.9	24.0	24.2	23.8	22.8	23.1	24.6	28.2	23.8	25.9	25.9	25.9			24.7±1.5	<.001								
PHYSIO		Δ_{tn-t0}	−0.2	−0.2	−0.4	−0.2	−0.7	−0.2	−0.4	0.1	−0.4	−0.2	0.0	−0.3					−0.3±0.2	<.001						
		t_0	33.0	33.1	32.7	34.9	32.8	32.7	32.7	33.7	32.7	32.6	31.5	32.6							32.9±0.8	<.001				
	C-C	t_n	33.1	33.1	32.7	34.8	32.8	32.6	32.8	33.9	32.9	32.9	31.7	32.9									33.0±0.8	<.001		
		Δ_{tn-t0}	0.0	0.0	0.0	−0.1	0.1	−0.1	0.2	0.1	0.1	0.2	0.2	0.3											0.1±0.1	.007
		t_0	29.2	32.1	28.0	27.5	29.8	26.2	33.3	32.6	32.6	30.6	28.7		30.1±2.4											
	S-L	t_n	27.9	31.4	24.8	25.8	27.9	27.1	31.1	30.5	31.1	27.5	27.0				28.4±2.3									
ETL-CTRL		Δ_{tn-t0}	−1.3	−0.7	−3.3	−1.7	−1.9	0.9	−2.3	−2.1	−1.6	−3.1	−1.7						−1.7±1.1							
		t_0	34.0	39.8	35.6	39.6	40.4	43.6	36.8	38.8	41.0	40.7	41.5								39.2±2.8					
	C-C	t_n	34.0	39.0	35.4	38.3	39.5	43.0	36.6	38.3	40.8	39.7	39.8										38.6±2.5			
		Δ_{tn-t0}	0.0	−0.7	−0.2	−1.3	−1.0	−0.7	−0.2	−0.5	−0.2	−1.0	−1.7												−0.7±0.5	
ETL	S-L	t_0	23.1	25.5	20.7	24.5	24.3	21.0	22.9	24.2	24.1	24.2	23.5		23.4±1.5	<.001										

			Animal no												Mean±1SD											
																	S-L						C-C			
			1	2	3	4	5	6	7	8	9	10	11	12	t0	P vs. CTRL	tn	P vs. CTRL	Δtn-t0	P vs. CTRL	t0	P vs. CTRL	tn	P vs. CTRL	Δtn-t0	P vs. CTRL
		t_n	23.6	25.3	20.5	23.1	23.9	20.8	22.7	23.9	24.0	24.0	23.1				23.2±1.4	<.001								
		$\Delta_{tn\text{-}t0}$	0.5	−0.1	−0.2	−1.3	−0.4	−0.1	−0.2	−0.4	−0.1	−0.2	−0.4						−0.3±0.4	.002						
		t_0	29.0	32.3	29.9	30.6	33.3	33.9	32.3	33.2	32.8	32.7	32.7								32.1±1.5	<.001				
	C-C	t_n	29.3	32.2	30.1	30.8	33.0	33.9	32.5	33.1	32.7	32.7	32.7										32.1±1.4	<.001		
		$\Delta_{tn\text{-}t0}$	0.3	−0.1	0.2	0.2	−0.2	0.0	0.2	−0.1	−0.2	0.1	0.0												0.0±0.2	.001
		t_0	27.6	29.8	26.0	29.8	27.5	27.2	31.1	29.6	30.9	28.3	24.8	30.1	28.6±2.0											
	S-L	t_n	25.8	28.5	25.2	27.9	23.5	23.2	29.0	26.6	27.0	27.6	22.8	28.1			26.3±2.2									
GEO-CTRL		$\Delta_{tn\text{-}t0}$	−1.8	−1.3	−0.9	−1.9	−4.1	−4.0	−2.2	−2.9	−3.9	−0.7	−2.0	−2.0					−2.3±1.2							
		t_0	36.6	34.8	34.2	35.7	36.6	36.8	38.3	38.5	42.5	41.0	37.4	43.0							37.9±2.9					
	C-C	t_n	35.1	35.2	33.2	34.9	33.9	36.2	37.9	37.8	40.4	40.0	36.4	41.7									36.9±2.7			
		$\Delta_{tn\text{-}t0}$	−1.5	0.4	−1.0	−0.8	−2.6	−0.6	−0.4	−0.7	−2.1	−0.9	−1.0	−1.3											−1.0±0.8	
		t_0	19.9	19.6	19.6	20.6	19.7	19.1	21.0	20.7	21.6	18.7	18.7	19.7	19.9±0.9	<.001										
	S-L	t_n	19.8	19.8	19.5	20.7	19.5	18.9	21.1	20.5	21.1	18.7	18.9	19.7			19.8±0.8	<.001								
GEO		$\Delta_{tn\text{-}t0}$	−0.1	0.2	−0.1	0.2	−0.3	−0.2	0.1	−0.2	−0.5	−0.1	0.2	−0.1					−0.1±0.2	<.001						
		t_0	33.4	33.4	31.5	34.9	34.8	33.7	35.8	36.5	35.7	35.4	35.7	36.2							34.7±1.5	.001				
	C-C	t_n	33.2	33.7	31.4	34.7	34.1	33.3	36.1	36.4	35.7	35.3	35.6	36.1									34.6±1.5	<.001		
		$\Delta_{tn\text{-}t0}$	−0.2	0.3	−0.1	−0.2	−0.7	−0.4	0.3	−0.1	0.0	0.0	−0.1	−0.1											−0.1±0.3	<.001

All values from individual animals are in mm and two beat averages, t_n=strained state (time point of maximum LVP), t_0=reference strain state (time point before mitral valve opening, see METHODS), COS=Edwards Cosgrove band, RSAR=St Jude Medical rigid saddle-shaped annuloplasty ring, ETL= Edwards IMR ETlogix, GEO=Edwards GeoForm, SD=standard deviation

TABLE 4

Global maximum principal (global ε_{max}), radial (global ε_{rad}) and circumferential (global ε_{cir}) strains

	Animal no													Mean±1SD					
		1	2	3	4	5	6	7	8	9	10	11	12	global ε_{max}	P vs. CTRL	global ε_{rad}	P vs. CTRL	global ε_{cir}	P vs. CTRL
	global ε_{max}	0.08	0.20	0.06	0.12	0.14	0.22	0.19	0.15	0.11	0.23	0.11	0.16	0.15±0.05					
COS-CTRL	global ε_{rad}	0.03	0.12	0.04	0.08	0.08	0.17	0.10	0.09	0.08	0.10	0.05	0.12			0.09±0.04			
	global ε_{cir}	0.04	0.11	0.04	0.05	0.07	0.08	0.07	0.09	0.04	0.07	0.03	0.10					0.07±0.03	
	global ε_{max}	0.19	0.19	0.07	0.13	0.14	0.14	0.15	0.14	0.12	0.16	0.12	0.21	0.15±0.04	.973				
COS	global ε_{rad}	0.08	0.15	0.05	0.10	0.11	0.11	0.06	0.09	0.09	0.13	0.07	0.12			0.10±0.03	.425		
	global ε_{cir}	0.08	0.08	0.04	0.05	0.07	0.04	0.08	0.06	0.05	0.10	0.03	0.13					0.07±0.03	.858
	global ε_{max}	0.08	0.19	0.24	0.08	0.18	0.09	0.17	0.16	0.08	0.14	0.07	0.14	0.14±0.05					
RSAR-CTRL	global ε_{rad}	0.04	0.15	0.20	0.05	0.10	0.03	0.10	0.16	0.04	0.09	0.05	0.07			0.09±0.05			
	global ε_{cir}	0.03	0.13	0.07	0.02	0.06	0.04	0.04	0.05	0.03	0.06	0.02	0.07					0.05±0.03	
	global ε_{max}	0.15	0.17	0.24	0.09	0.21	0.09	0.18	0.18	0.10	0.15	0.09	0.23	0.16±0.05	.024				
RSAR	global ε_{rad}	0.12	0.15	0.20	0.06	0.12	0.06	0.15	0.17	0.03	0.10	0.06	0.16			0.11±0.05	.010		
	global ε_{cir}	0.06	0.09	0.09	0.05	0.11	0.05	0.07	0.04	0.06	0.06	0.05	0.11					0.07±0.02	.022
	global ε_{max}	0.17	0.15	0.19	0.20	0.17	0.12	0.16	0.14	0.18	0.09	0.11	0.17	0.15±0.03					
PHYSIO-CTRL	global ε_{rad}	0.11	0.04	0.08	0.09	0.14	0.04	0.12	0.08	0.10	0.03	0.07	0.13			0.08±0.04			
	global ε_{cir}	0.05	0.11	0.11	0.09	0.07	0.08	0.06	0.07	0.03	0.03	0.05	0.07					0.07±0.03	
	global ε_{max}	0.21	0.18	0.21	0.19	0.20	0.12	0.20	0.20	0.14	0.14	0.11	0.24	0.18±0.04	.020				
PHYSIO	global ε_{rad}	0.14	0.03	0.10	0.13	0.14	0.04	0.14	0.11	0.09	0.04	0.05	0.13			0.09±0.05	.102		
	global ε_{cir}	0.10	0.13	0.10	0.10	0.10	0.05	0.11	0.13	0.04	0.08	0.06	0.15					0.10±0.03	.010
ETL-CTRL	global ε_{max}	0.21	0.08	0.09	0.12	0.07	0.10	0.07	0.08	0.09	0.20	0.06		0.11±0.05					

	Animal no													Mean±1SD				
		1	2	3	4	5	6	7	8	9	10	11	12	global ε_{max}	P vs. CTRL	global ε_{rad}	P vs. CTRL	global ε_{cir}	P vs. CTRL
	global ε_{rad}	0.15	0.07	0.06	0.11	0.02	0.04	0.04	0.07	0.03	0.15	0.03				0.07±0.05			
	global ε_{cir}	0.13	0.02	0.03	0.05	0.05	0.06	0.04	0.03	0.02	0.12	0.03						0.05±0.04	
	global ε_{max}	0.19	0.11	0.17	0.24	0.06	0.11	0.15	0.11	0.12	0.17	0.09		0.14±0.05	.042				
ETL	global ε_{rad}	0.10	0.08	0.08	0.17	0.03	0.03	0.05	0.10	0.07	0.11	0.06				0.08±0.04	.349		
	global ε_{cir}	0.14	0.05	0.11	0.12	0.04	0.08	0.07	0.04	0.05	0.09	0.06						0.08±0.03	.017
	global ε_{max}	0.13	0.15	0.04	0.17	0.06	0.08	0.19	0.17	0.11	0.13	0.16	0.13	0.13±0.05					
GEO-CTRL	global ε_{rad}	0.08	0.10	0.02	0.12	0.02	0.03	0.08	0.11	0.06	0.09	0.06	0.07			0.07±0.03			
	global ε_{cir}	0.07	0.10	0.01	0.07	0.02	0.02	0.11	0.03	0.07	0.05	0.05	0.06					0.06±0.03	
	global ε_{max}	0.14	0.21	0.05	0.22	0.16	0.07	0.17	0.20	0.16	0.16	0.18	0.19	0.16±0.05	.009				
GEO	global ε_{rad}	0.07	0.15	0.01	0.12	0.09	0.04	0.05	0.14	0.07	0.05	0.00	0.11			0.07±0.05	.581		
	global ε_{cir}	0.09	0.11	0.02	0.13	0.02	0.02	0.08	0.04	0.10	0.07	0.07	0.07					0.07±0.04	.065

All values from individual animals are two beat averages, COS=Edwards Cosgrove band, RSAR=St Jude Medical rigid saddle-shaped annuloplasty ring, ETL= Edwards IMR ETlogix, GEO=Edwards GeoForm, SD=standard deviation